Droplet Trajectories of Wave Impact Sea Spray on a Marine Vessel

S.R. Dehghani[1], Y.S. Muzychka, G.F. Naterer

Department of Mechanical Engineering, Faculty of Engineering and Applied Science,

Memorial University of Newfoundland, St. John's, NL, A1B 3X5, Canada

Abstract

Marine icing phenomena are strongly dependent on the rate of water impact on marine vessels. The most important component is wave-impact sea spray. There is limited understanding of droplet size and velocity distributions of wave-impact sea spray. Initial distributions of size and velocity of droplets are crucial for the calculation of the droplet path and consequently for determining the water impact on surfaces. This paper develops a new model of wave-impact sea spray by using a distribution of the size and velocity of droplets at the edge of the vessel. The concepts of water-sheet breakup and droplet breakup lead to an inverse dependence between the size and velocity of droplets after the breakup process. Droplets take different paths and form a spray cloud in front of the vessel. The liquid water content in front of the vessel can be calculated by considering the arrangement, sizes, and velocities of a set of droplets in the spray cloud. The response of the droplet trajectory model to various initial conditions with different sets of droplet sizes and velocities is examined. The numerical results are compared to real data from field observations. Droplet sizes are inversely proportional to droplet velocities, as verified by liquid water content data obtained by the field observations. This paper proposes the use of this inverse relationship based on physics of the breakup process, as the initial data for calculating the wave-impact sea spray trajectory in front of a vessel.

Keywords: Marine Icing, Wave Impact, Sea Spray, Droplet Trajectory, Sheet Breakup, Droplet Breakup

---

[1] Corresponding author, Postdoctoral Fellow, Phone: +1 (709) 771-6216, Email: srdehghani@mun.ca

23

1. Introduction

25 Marine icing phenomena, involving ice accretion and accumulation on vessels, have been significant

26 challenges in offshore technology development. Due to growing expectations about the role of the Arctic

27 in supplying oil and natural gas resources, the importance of marine icing phenomena has increased.

28 Accurate prediction of ice accretion on marine vessels has remained a challenging concern. Researchers

29 have made many efforts in this field, but several aspects of these phenomena are not yet well understood

30 (Kulyakhtin and Tsarau, 2014; Shipilova et al., 2012; Ryerson, 2011).

31   Atmospheric and sea-generated droplets are two sources of water droplet delivery. Field

32 observations show that atmospheric droplets and humidity, including rain, snow, drizzle, and fog, are not

33 the most significant contributors to ice accretion, and consequently, they are not the main potential

34 causes for ice accretion on marine objects in harsh conditions. These have been analysed in detail by

35 Makkonen (1984). On the other hand, sea-generated water droplets have more significant roles in the

36 occurrence of ice creation and accumulation on marine objects (Lozowski et al., 2000; Zakrzewski, 1987).

37 Wind-generated spray, which refers to droplets raised from the sea surface by wind, and wave-impact-

38 generated spray, caused by atomized droplets created by wave impact on the outer surface of marine

39 objects, are two important sources of sea-generated droplets. Wind-generated droplets generally have

40 lesser effects on marine icing phenomena, and they are often neglected in the calculations of ice accretion

41 (Lozowski et al., 2000; Zakrzewski, 1987). Wave-impact-generated droplets are the main cause of ice

42 accretion on marine objects. In harsh conditions at sea, marine vessels are faced with a high rate of water

43 impact due to the differing impacts of high-energy waves (Zakrzewski, 1987). Figure 1 shows a general

44 schematic of the sources of the water droplets delivered to marine vessels and their role in marine icing
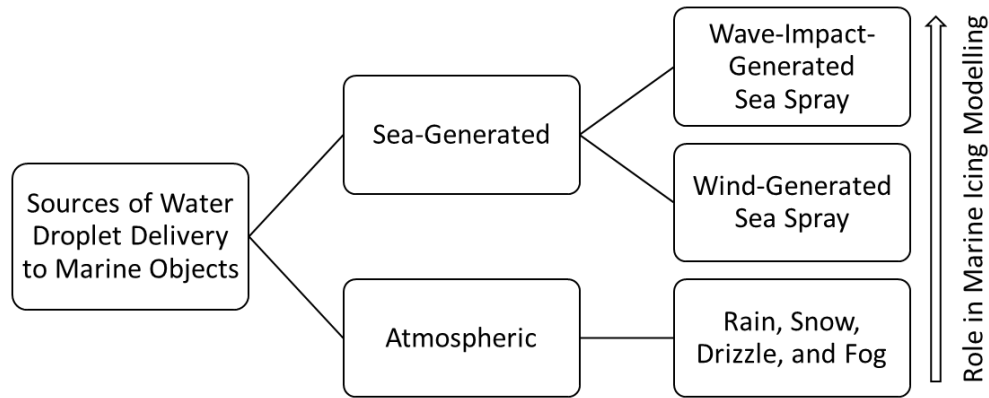
45 modeling.

46

47

48   Fig. 1. Sources of water impact and their role in marine icing modelling

49

50   A review of previous studies shows that there are limited field observations or the measurement

51   of the rate of water delivery to marine objects due to wave impact. Some correlations and empirically-

52   based relations have been developed. These relations describe the rates of incoming water of a wave-

53   impact sea spray, which are usually the amounts of water in a unit volume of air, called the Liquid Water

54   Content (LWC). The most significant investigations of wave-impact sea spray are from Borisenkov et al.

55   (1975), Zakrzewski (1987), Horjen and Carstens (1989), and Ryerson (1995). These attempted to extract

56   LWC data from field observations. The vertical distributions for liquid water content have been the most

57   useful data obtained from the field observations. These LWC relations have been used by researchers to

58   predict ice accretion on vessels.

59   The main focus of this paper is on wave-impact sea spray in front of vessels. There have been a

60   few past works which are directly related to vessels. Borisenkov et al. (1975) showed that the LWC, which

61   results from wave-impact splashes, varies by height from deck level exponentially. The correlation and

62   model were based on observations in the Sea of Japan obtained by a Medium-sized Fishing Vessel (MFV).

63   It reported the amount of incoming water to the deck without reporting the size and velocity of droplets.

64   The report of Borisenkov et al. (1975) was the first and most significant investigation which is related to

65   vertical distribution of LWC in front of a vessel.

3

66   Zakrzewski (1987) extended the work of Borisenkov et al. (1975) by generalizing the correlation

67   for all wave conditions. It was assumed that the LWC depends on wave height and that the relative velocity

68   of a wave and vessel can increase the LWC by a power of one and two respectively. The generalized

69   relation was verified by Borisenkov's correlation. Ryerson (1995) included aspects of droplet size

70   distribution and droplet concentration for wave-impact sea sprays. The observations showed that there

71   is a range of droplet diameters from very fine, at 14 μm, to very large, at 7,700 μm. In addition, it was

72   reported that the mean droplet concentration was $4 \times 10^5 \ drops/m^3$. This gives more information than

73   the liquid water content alone.

74   Calculations and predictions of ice accretion on a surface are strongly dependent on the rate of

75   water droplet impact at every location of that surface on marine vessels. The rate of water droplet delivery

76   depends on droplet trajectories from the injection spots, which are the upper edges of the vessel bow, to

77   target surfaces. The gravity force, wind velocity, initial size of droplets, initial velocity of droplets, and

78   many other parameters can affect droplet trajectories and, consequently, the rate of water received on

79   target surfaces (Zakrzewski and Lozowski, 1988). The crucial data for applying a droplet trajectory analysis

80   are droplet size distribution, droplet velocity distribution, and droplet concentration (Dehghani et al.,

81   2009). With this information, the geometry of the vessels or offshore structures, and some atmospheric

82   information, a good estimation of sea water droplet delivery to the surface points can be predicted.

83   Therefore, without a sophisticated model for the distribution of the droplet sizes and velocities, it is

84   difficult to accurately predict the rate of droplet water impingement on target surfaces; as a result, the

85   estimate of the amount of accumulated ice will not be accurate.

86   Past studies have reported relations that explain the vertical distribution of LWC due to the impact

87   of waves on vessels and offshore superstructures (Forest et. al, 2005; Zakrzewski, 1987; Lozowski et al.,

88   2000). These involve functions of wave specifications, atmospheric situations and marine object

89   characteristics. Estimating the accumulated ice needs the contribution of the droplet trajectory method

4

90   to give a good estimation of water impact on the surface. Past studies have typically assumed droplet

91   sizes, velocities, and concentrations in order to calculate the droplet trajectories and, consequently, the

92   ice accretion results. Lozowski et al. (2000) used a RIGICE model and assumed the initial vertical and

93   horizontal velocities and initial drop sizes. Other researchers who used the droplet trajectory have not

94   used distributed droplet sizes and droplet velocities. They usually assumed a fixed initial velocity and size

95   for all heights (Shipilova et al., 2012; Horjen, 2013; Kulyakhtin and Tsarau, 2014).

96   The complete set of data of wave-impact sea spray should include the distribution of droplet size,

97   velocity, and concentration. To date, there has been no past work to describe a wave-impact sea spray by

98   considering this essential information. In addition, phenomena related to the creation of the wave-impact

99   sea spray have not yet been explained (Zakrzewski, 1987; Lozowski et al., 2000; Shipilova et al., 2012;

100   Horjen, 2013; Kulyakhtin and Tsarau, 2014).

101   Ryerson (1995) reported the size and concentration of droplets. This was based on the measured

102   samples from some regions of a spray cloud and not a complete distribution data set for the whole spray

103   cloud. The user would need to generalize the suggested distribution for the droplet size and concentration

104   to all regions of the spray cloud. In addition, having an initial velocity distribution for droplets is crucial to

105   obtain the path of a spray cloud on the vessel and Ryerson's model did not include the droplet velocity

106   data.

107   There have been previous investigations into determining the LWC for offshore structures. In

108   those cases, the geometry of the surfaces that waves impact is different from the vessel's bow. Their

109   wave-impact sea spray would be different. Forest et al. (2005) reviewed past LWC relations for offshore

110   structures. The exponential form of those relations is the same as the relations for the vessels but they

111   have some significant differences. As mentioned, the most relevant formula for the vertical distribution

112   of LWC for vessels is a model of Borisenkov et al. (1975), and developed by Zakrzewski (1987). The formula

113   presented by Borisenkov et al. (1975) is one of the formulae based on real field observations in the Sea of

114 Japan by using the MFV. It is at least valid for that special situation, that vessel geometry, and the

115 environmental situation.

116   In the present work, a new correlation between droplet sizes and velocities at the injection area,

117 the top edge of the bow, is introduced. This size-velocity dependence for droplets aids in the use of the

118 LWC information. The new model will be examined in comparison with the LWC from field observations

119 for real vessels (Borisenkov et al. 1975), and a sensitivity analysis will show the effect of various

120 parameters on the output of the model.

121

122 2. Wave-Impact Sea Spray

123 Dividing the marine icing phenomena into two consequent phenomena, called *off-deck* and *on-deck*

124 phenomena in this study, will clarify the importance of wave-impact sea spray. The off-deck phenomena

125 are those that occur outside of the marine vessel. These include sea wave creation and movement, sea

126 wave impact on marine objects, water breakup, and finally droplet dispersion in front of the marine

127 object. This set of distributed water droplets in front of a vessel is called wave-impact sea spray. On the

128 other hand, the on-deck phenomena are those which occur on and above the marine objects. The spray

129 and droplet trajectory, droplet impingement to marine objects, start of icing, and ice accretion are the

130 main subdivisions of the on-deck phenomena.

131   The majority of past research has been focused on on-deck phenomena. There have been many

132 reports on ice accretion, which is the final stage of on-deck phenomena. But there is a limited number of

133 studies about the impact of sea water droplets on vessels. It should be noted that the quality and accuracy

134 of the prediction of ice accretion is strongly dependent on the rate of incoming water droplets on marine

135 vessels. The estimation of off-deck phenomena is a prerequisite for accurate prediction of on-deck

136 phenomena. But off-deck phenomena are lesser-known parts of the marine icing phenomena. Figure 2

137 illustrates the classification of marine icing phenomena based on the above-mentioned description.

138
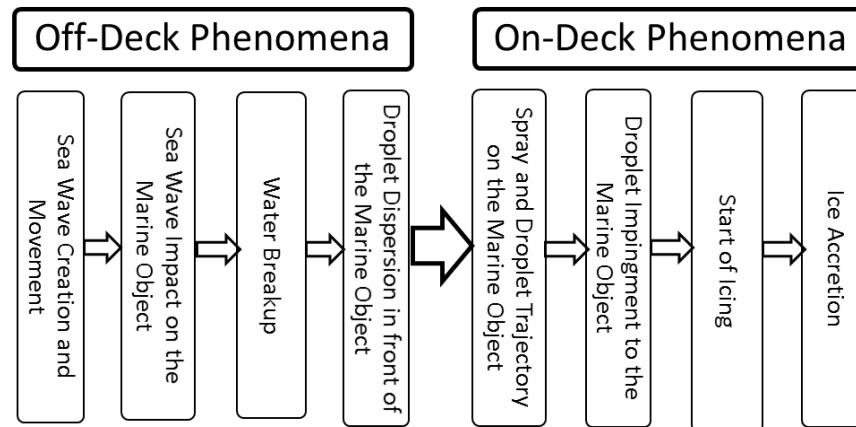
Fig. 2. Classification of wave-impact marine icing phenomena

139

140

141

142   A review of past research related to wave–impact sea spray for a vessel's bow shows that this

143   field of research was initially pursued with field observation data (Borisenkov et al., 1975). There are

144   variations of LWC for various heights, vessel speeds, heading angles, wind speeds, wave specifications,

145   sea water temperatures, wind temperatures and some other information related to the icing situation.

146   These were examined by Zakrzewski (1987) and Lozowski et al. (2000) by generalizing a specific correlation

147   to various situations. Information about LWC is not sufficient for estimating the rate of water impact on

148   every point of a vessel. Size, velocity and concentration of the droplets are the other elements that are

149   required for the droplet trajectory. There have been some attempts to find a good estimation of size and

150   velocity of droplets in a cloud of wave-impact sea spray. However, none can yield a distribution of size

151   and velocity of the droplets in front of a vessel. Some of these attempts assumed the velocity of droplets

152   to be the same as the wind velocity. In MARICE, the initial velocity, which is related to the wave

153   specification and heading angle, was proposed as a model (Lozowski et al., 2000; Shipilova et al., 2012;

154   Horjen, 2013; Kulyakhtin and Tsarau, 2014). None of the previous works used a distribution of droplet size

155   as initial sizes for droplet trajectories (Zakrzewski, 1987; Lozowski et al., 2000; Shipilova et al., 2012;

7

156   Horjen, 2013; Kulyakhtin and Tsarau, 2014). Therefore it is important to have a good estimation of the

157   distribution of droplet size and velocity to be able to use the droplet trajectory method and calculate the

158   rate of water delivery to every point of a vessel.

159   Droplet sizes and velocities are a result of the breakup of sea water. Evaluating this breakup

160   mechanism leads to a relation between droplet sizes and velocities. In the present paper, the vessel bow

161   is chosen as a sample of an inclined surface that has the potential for conducting water-sheet breakup.

162   The other points of the vessel which are in direct contact with seawater have a similar potential for

163   creating a wave-impact sea spray. Impacting waves on those regions can cause water breakup and droplet

164   creation which will create the cloud of wave-impact sea spray.

165   The wave impact on a vessel bow is the starting step of sea-spray cloud formation. Similar to other

166   impacts of water on vertical or inclined rigid surfaces, an upward thin water sheet is expected to form on

167   the bow. The local impact velocity of the water particles on the bow is one of the main criteria for the

168   quality of the thin water sheet creation. It determines the velocity and thickness of the water sheet. This

169   sheet of water can slip on the bow or separate from the bow at an angle. In case of low-velocity impact

170   and the consequent low velocity of sheets, the sheet water may stay unified and continue its movement.

171   High-velocity impacts can create a high-velocity water sheet leading to surface breakup and,

172   consequently, to droplet breakup. High-velocity sheets cannot keep unity, and they break into many small

173   parts. Long water strips are one result of sheet breakup and water droplets are the final result of the

174   secondary breakup. The most important stages of wave-impact sea spray phenomena are shown in Fig. 3.

175
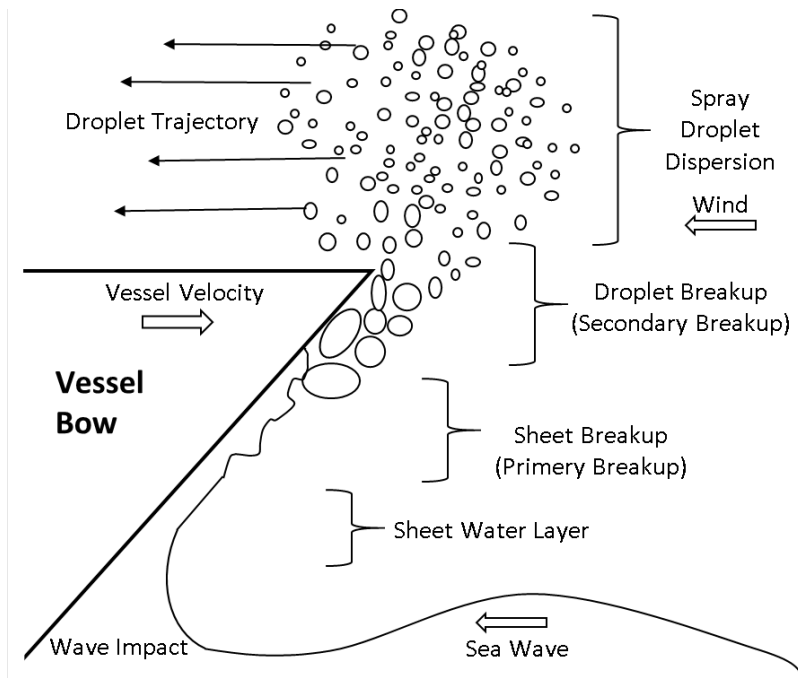
176

177   Fig. 3. Illustration of the wave impact, water sheet creation, and breakup stages

178

179   The stages are, in order: wave impact on the bow, water sheet creation on the bow, sheet

180 breakup, droplet breakup, and droplet dispersion in front of the vessel. The last stage is known as a sea

181 spray cloud in front of the vessel. The wind velocity, vessel velocity, and the other contributors to this

182 process are shown in Fig. 3.

183   The impact of a single sea wave on a bow occurs at various velocities. Impact velocity is the

184 relative velocity of water particles with respect to the bow in the contact area. Due to the variation of

185 contact areas, and different local velocities of water particles of the wave, the impact velocity will be

186 variable. It is worth considering that, in the short period of the impact, the velocity of the impact varies

187 from a minimum effective velocity to a maximum supplied velocity. The minimum effective velocity is the

188 minimum velocity that is required for the creation of a sheet of water. The maximum supplied velocity is

189 the maximum velocity of impact that is possible to occur between the wave and vessel. This behaviour of

190 velocity variation makes spray-cloud modelling more complex.

9

191   In some cases, the impact velocity is sufficient to create a sheet of water in effective periods of

192   impact. The impact velocity must be high to to create a thin sheet of water on the bow. In the short

193   effective period of impact, the bow experiences a range of impact velocities that make various sheets of

194   water on the bow. A sheet of water is formed on the bow because the water particles of the wave have

195   enough energy to overcome gravity. Sometimes a sheet of water is formed, but the breakup does not

196   occur. This implies that there are more criteria involved in the breakup phenomenon (Ahmed et al., 2009).

197   Breakup occurs when two portions of fluid or a single portion of fluid forms a free surface with

198   surface energy. A system which is not at the minimum level of energy will attempt to rearrange and move

199   toward the lower energy level, leading to the breakup of the fluid into smaller portions to minimize the

200   system surface energy by reducing the surface area. The exact outcome of the breakup process is

201   dependent on the surface tension, viscosity, density, and diameter of the thread undergoing breakup. In

202   other words, breakup will occur when inertia forces, which are representatives of density, velocity and

203   diameter, can be controlled by surface tension forces. In this case, existing instabilities can grow and

204   create water strips and droplets (Sazhin 2014). Some of the sheet conditions on the bow may be able to

205   satisfy the criteria of water breakup and atomization. In this case, the breakup starts to split the water

206   sheet into smaller parts.

207   High-velocity air flow, in the presence of the liquid sheet water on the bow, can create significant

208   shear development at the interface between the two fluids. The shear gives rise to a Kelvin-Helmholtz

209   type instability, causing the sheet to be disturbed, and as the oscillating amplitude grows, the sheet will

210   split into divided parts. Stretching causes the sheet to tear into ligaments. The breakup mechanisms

211   appear to be independent of the water viscosity and surface tension; however, these properties affect

212   the final drop size distribution (Lozano et al. 1998).

213   As mentioned, the impact velocity is not constant. Therefore, the sheet velocity and the resultant

214   droplet velocities are not constant (Sarchami et al. 2010). In every single impact, the bow is faced with a

215   range of impact velocities that create various sheet velocities and therefore, various sizes of droplets.

216   Low-velocity impacts make big droplets with a low velocity; these droplets are stable and cannot be

217   further divided. The high-velocity droplets are unstable and split into smaller droplets. They continue their

218   division to reach a stable condition, involving a balance between the inertia and surface tension at the

219   end of the breakup process. The sizes of the droplets depend on their velocities: higher velocities lead

220   droplets to resize to finer droplets, while the medium velocity droplets may split up into medium-sized

221   droplets. Therefore, at the end of droplet breakup there are various sizes of droplets with different

222   velocities: the bigger droplets have low velocities and the smaller droplets have high velocities (Sazhin

223   2014). Figure 4 shows the size-velocity dependence of droplets at the end of the breakup procedure.

224
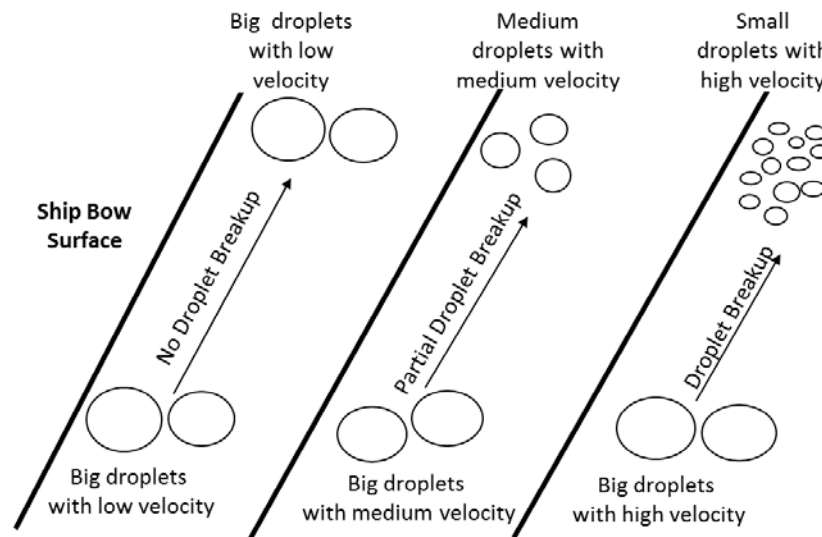
225

226   Fig. 4. Three types of droplet breakup mechanisms and size-velocity dependence

227

228   After the breakup stage, the droplets continue their paths in front of the bow. At this time, the

229   wave-impact sea spray is visible and a spray cloud appears in front of the vessel. The forces exerted on

230   the droplets determine the quality of the spray trajectory. The most important forces are body force, drag

231   force, and added mass force (Dehghani et al. 2009). These forces reduce the droplet velocity and move

232   them to change their direction and travel in the direction of the wind and gravity. Aspects of this

233   procedure can be calculated by using the droplet trajectory method in front of the vessel.

234   In past research, sea spray creation due to bow-wave interaction has not been well understood.

235   The main interest of studying bow-wave interaction has been the calculation of the force exerted on the

236   bow or the amount of direct water on the deck (Gu et al. 2014; Greco and Lugni, 2012; Greco et al., 2012;

237   Kapsenberg, 2011). There is a similar phenomenon that can be used for understanding these stages. Sheet

238   breakup on a rigid surface has been investigated in splash plates by several researchers. A splash plate

239   creates splash and spray droplets by using the impact of water on an inclined surface plate (Ahmed et al.

240   2009; Bussmann et al., 2000; Sarchami et al., 2010; Ashgriz et al., 1996). This procedure includes sheet

241   water breakup and droplet breakup, which are fundamentally very similar to the breakup mechanisms on

242   the bow.

243
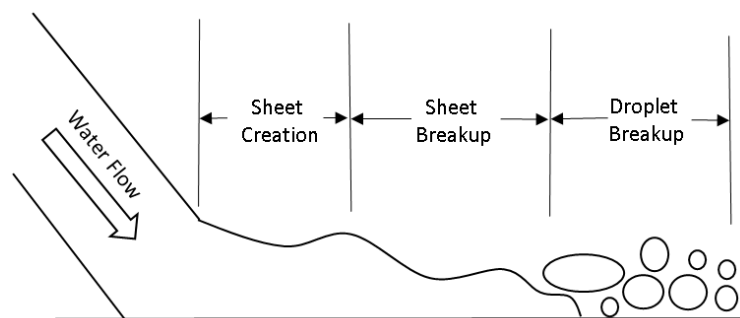
244

245   Fig. 5. Schematic view of a splash plate

246

247   In splash plates, the droplet velocity at the end of the plate depends on the initial velocity of the

248   water impact on the plate. In addition there is a dependence between the velocity and size of the

249   produced droplets. Experimental results show that there is an inverse dependence between the velocity

250   and size of the droplets at the end of the plate; this means that droplets with bigger sizes have lower

251   velocities in comparison to the small droplets (Sarchami et al., 2010). This fact is not only applicable to the

252   splash plates; it is the physical mechanism of liquid breakup and atomization. The fundamental physics of

253   liquid breakup maintains that the free surface liquid with a high velocity must break up into smaller sizes.

254   The theory of atomization states that low-velocity liquids can retain their unity, but the other high-velocity

255   parts are divided and resized to satisfy the balance of inertia and surface tension forces. The Weber

256   number is the common parameter for the breakup process and it can explain this inverse dependence

257   easily (Sazhin, 2014).

258   Sarchami et al. (2010) showed that for a splash plate, the droplet velocity and size have an inverse

259   relationship. The research demonstrated that increasing the initial velocity from $10\ m/s$ to $30\ m/s$ creates

260   droplets of about 350 μm to 250 μm in diameter, respectively; therefore, increasing velocity produces

261   finer droplets and consequently the high-velocity droplets are small in size and vice versa.

262   There have been several studies on the size and velocity of droplets for sheet and droplet breakup.

263   These studies indicate that this relation is inverse. According to the breakup situation and associated

264   parameters, and considering the dominant mechanism of breakup, this inverse relation can vary. Adams

265   et al. (1977) suggested a correlation for droplet sizes of a sheet breakup process as follows:

266                              $$D \times V^{0.55} = constant$$ (1)

267   where D and V are the droplet diameter and velocity respectively. The *constant* depends on the viscosity,

268   surface tension, and density of the sheet, and also on dimensional characteristics which are fixed for a

269   breakup process. In this relation, droplet diameters are inversely proportional to the 0.55th power of

270   droplet velocities.

271   In Ingebo's work (1984), which is experimental, an empirical correlation for droplet size and

272   Reynolds number is resented. The correlation is as follows:

273                              $$D \times V = constant$$ (2)

274   The *constant* depends on the viscosity and density of the sheet and also the geometry of the plate. This

275   paper proposes another inverse dependence between the sizes and velocities of the droplets.

276   The droplet breakup is the other breakup mechanism which contributes to this process. Bag

277   breakup, which is a type of breakup in which droplets are split up after formation of a water bag, and

278   stripping breakup, which is splitting droplets by the contribution of surface shear force between air and

279   water, can be two dominant mechanisms in this stage. The Weber number is a useful criterion for

280   assessment of the breakup situation. According to Sazhin (2014), the Weber number, which is the criterion

281   for bag breakup, can be shown as follows:

282
$$We = \frac{\rho V^2 D}{\sigma} \tag{3}$$

283   where ρ is air density, σ is surface tension, and We is the Weber number. In the breakup condition, the

284   surface tension and air density are considered constant. The breakup process is stopped when the Weber

285   number reaches lower than a critical amount. Therefore, the Weber number for the end of the breakup

286   process is considered constant and consequently, a new relation can be developed:

287
$$D \times V^2 = constant \tag{4}$$

288   The *constant* depends on the surface tension, density and the Weber number. This inverse dependence

289   occurs by a power of two.

290   The other probable mechanism of breakup is stripping breakup (Sazhin, 2014). The criterion for

291   this type of breakup is suggested in terms of $We/\sqrt{Re}$. or after manipulation,

292
$$D \times V^{1.5} = constant \tag{5}$$

293   The *constant* depends on the surface tension, viscosity, density and the Weber number. In this relation,

294   droplet diameters are inversely proportional to the 1.5th power of the droplet velocities.

295   As mentioned above, the overall mechanism of breakup in wave-bow impact is a mixture of sheet

296   breakup and droplet breakup. Also there is an overall inverse dependence between the velocity and size

297   of the droplets at the end of the breakup process, and the quality of this inverse proportion depends on

298   the breakup conditions. Equations (1, 2) and (4, 5), which are the samples of size-velocity relations,

299 confirm this overall inverse dependence. Other past research on the breakup process confirms this fact

300 as well (Sazhin, 2014).

301 The above equations emphasise that at the end of the water breakup process, the bigger droplets

302 have a lower velocity in comparison to the smaller droplets. The magnitude of velocity and size and the

303 power of that inverse proportion depends on the details of the breakup mechanism. This observation is a

304 significant fact that can be used for reaching a distribution of size and velocity of droplets in front of a

305 vessel's bow. The power of that proportion varies around unity and the exact overall power cannot be

306 found easily. The inverse proportion, however, is more important than the exact amount of the power. In

307 this paper, we will assume that the overall breakup phenomenon is an average of those phenomena, and

308 based on this assumption, the sizes and velocities are obtained and used.

309

310 3. Droplet Trajectory Analysis

311 Spray droplets are expected to move upward next to the bow and be injected into the free stream above

312 the bow tip in front of the vessel. The droplets are injected with various velocities and masses. Their kinetic

313 energies are different, and some of the droplets with a higher level of kinetic energy can travel in front of

314 the vessel, while others do not have enough kinetic energy to overcome gravity acceleration and will

315 quickly return to the sea. Very big and low-velocity droplets will return to the sea and the rest will meet

316 the free stream.

317 Droplets are injected into the air stream in a direction which is nearly parallel to the bow. This

318 means they enter the air stream in the opposite direction of the force of the gravity and also in the

319 opposite direction of the wind velocity. Droplets are decelerated by the air stream and gravity and

320 consequently change their direction to the wind direction and downward direction. The trajectory of the

321 droplets in front of the vessel is modeled by the one-way modeling method and solved by a numerical

322   method. By assuming a uniform flow in the direction opposite that of the vessel, and knowing the droplet

323   size and velocity, solving the spray trajectory becomes possible.

324   Spherical droplets, having a density of ρ_d and a diameter of D_d, which is very small compared to

325   the flow length scale (the bow dimension), are assumed. Applying Newton's Second Law for the droplet

326   motion and substituting the body force, drag force, and added mass force, will result in the governing

327   equation of the droplet trajectory. The governing equation related to droplet movement and the forces

328   acting on them can be derived as follows (Dehghani et al. 2013):

329
$$m_d \frac{dV_d}{dt} = \rho_d \forall_d \mathbf{g} - C_{dr} \frac{\pi D_d^2}{8} \rho_a |V_d - V_a|(V_d - V_a)$$

330
$$+ \rho_a \forall_d C_{ad} \frac{D(V_a - V_d)}{Dt} + \rho_a \forall_d \left(\frac{DV_a}{Dt} - \mathbf{g} \right) \tag{6}$$

331   where m_d is mass of droplet, t is time, V_d is droplet velocity, V_a is air velocity, ρ_d is water density, $\forall_d$ is

332   droplet volume, $\mathbf{g}$ is gravity, C_{dr} is drag coefficient, D_d is droplet diameter, ρ_a is air density, and C_{ad} is

333   added mass force coefficient. The coefficient C_{ad} is assumed 0.5 and C_{dr} can be calculated as follows

334   (Dehghani et al. 2009):

335
$$C_{dr} = \begin{cases} \dfrac{24}{Re} & Re < 1 \\ \dfrac{24}{Re}(1 + 0.15Re^{0.687}) & 1 < Re < 1000 \\ 0.44 & Re > 1000 \end{cases} \tag{7}$$

336   In order to solve this equation, its unknowns are calculated separately. Substituting the unknowns

337   leads to a set of ordinary differential equations.

338
$$\dot{x} = \frac{dx}{dt}, \qquad \ddot{x} = \frac{d^2x}{dt^2}, \qquad \ddot{x} = -\frac{3C_{dr}}{4D(\gamma + C_{ad})}(\dot{x} - U)\sqrt{(\dot{x} - U)^2 + \dot{z}^2} \tag{8}$$

339
$$\dot{z} = \frac{dz}{dt}, \qquad \ddot{z} = \frac{d^2z}{dt^2}, \qquad \ddot{z} = \left(\frac{1-\gamma}{\gamma + C_{ad}} \right)\mathbf{g} - \frac{3C_{dr}}{4D(\gamma + C_{ad})}(\dot{z})\sqrt{(\dot{x} - U)^2 + \dot{z}^2} \tag{9}$$

340   where $x, \dot{x}, \ddot{x}, z, \dot{z},$ and $\ddot{z}$, are position, velocity, and acceleration of the droplets, γ is liquid density to air

341   density ratio, and U is the relative velocity of wind to vessel. The initial conditions are droplet sizes and

342   velocities. This set of six equations and six unknowns can be solved by a numerical scheme.

343   The contribution of latent heat means that the amount of vaporization is important in the cooling

344   of the droplets, but in reality the mass of vaporized water is negligible in comparison to the original mass

345   of the droplets. Therefore, the small mass reduction due to the vaporization is ignored. The numerical

346   solution is limited to modeling of the droplet trajectory just in front of the vessel. Droplets traveling on

347   the deck are dependent on the vessel geometry and obstacles on the deck, which is beyond the scope of

348   this paper.

349   The input data for the droplet trajectory model are wind velocity, injection angle, droplet sizes and

350   droplet velocities. The present model simulates the wave-impact sea spray that MFV on the Sea of Japan

351   experienced (Borisenkov et al., 1975), and therefore in this work the situation of that vessel and the

352   atmospheric conditions of that time will be used in the analysis. The wind velocity is considered to be the

353   same as the MFV on the Sea of Japan. The range of droplet sizes is chosen by using the work of Ryerson

354   (1995) which is about 0-7000 μm. The initial velocities must be chosen to create a spray height recorded

355   in the same as the report of the MFV of the Sea of Japan (Borisenkov et al., 1975). By having a specific

356   amount of sea water that creates the cloud of spray and also having a distribution of size and velocity of

357   the droplets, the concentrations of droplets are determined. The injection angle will be assumed as the

358   overall injection angles of droplets after the sheet-water breakup. In a steady state situation, this angle

359   can be considered equal to the bow angle. The real phenomenon is transient, and the hitting angle of the

360   wave and bow occur such that the oscillation of the vessel will result in different injection angles.

361   Therefore the injection angle can be assumed about the bow angle and by considering a reasonable

362   tolerance, the variation of that angle can be addressed.

363   By using a range of velocities and sizes for droplets and considering the inverse relations for sizes

364   and velocities, a set of curves can be plotted. Figure 6 shows the distribution of the size and velocity of

365   droplets for a droplet range of 0-7000 μm and a velocity range of 0-40 m/s. The bottom-right corner of

366   Fig. 6 illustrates small and high-velocity droplets. Although the droplets can theoretically attain high

17

367   velocities, the drag force, which is a contraflow force, slows them down rapidly. The length scale of the

368   bow is bigger than the length scale of the splash plate and thus the effect of drag force in reducing the

369   velocity of high-velocity droplets will be more considerable than the splash plates. In reality, the high-

370   velocity and small droplets will be affected by this drag force and as a result it reduces their velocities at

371   a short distance from the creation area. Therefore, this is a reasonable assumption to correct the high-

372   velocity region and limit it to the maximum velocity. This correction shifts the right-hand half of the curves

373   of Fig. 6 a little lower. In moving more towards the higher velocity region, this shift will be more

374   considerable.

375
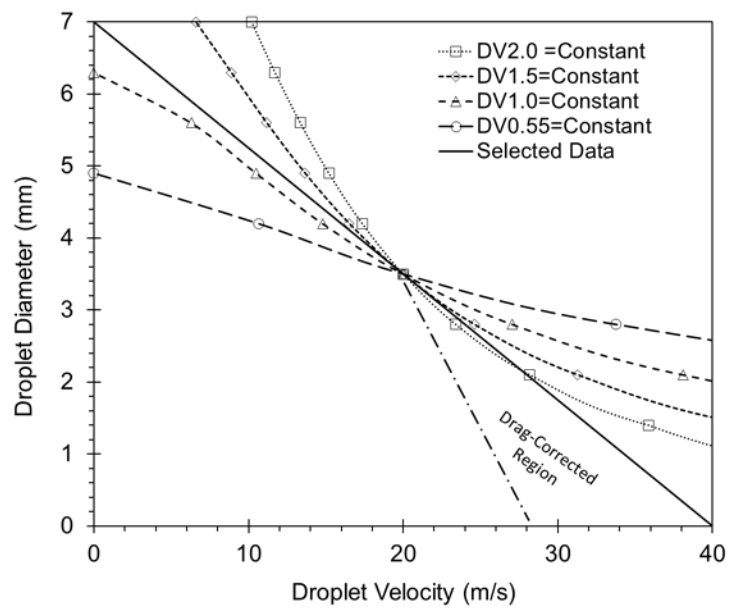
376

377   Fig. 6. Sample of size-velocity dependence for droplets

378

379   The breakup phenomenon can have combinations of some breakup mechanisms that have been

380   explained. Figure 6 shows the effects of those mechanisms on the size and velocity of the droplets. It is

381   difficult to determine that just one of those mechanisms is effective in determining the sizes and

382   velocities. All of them can contribute to forming the cloud of spray. It is reasonable to assume approximate

18

383 overall results for those outputs. A simple inverse size-velocity dependence which is chosen in this study

384 and named as *selected data* is the linearly decreasing line in Fig. 6. This inverse dependence curve covers

385 the weakness of the other models in the high-velocity region. It also reflects the overall effects of the

386 other models in the low-velocity and big-sized regions.

387

388 ## 4. Numerical Results

389 In a wave-impact spray event, size and velocity distributions of the droplets are essential for determining

390 the exact rate of water delivery to every part of a vessel. Previous research has shown that the droplet

391 size and velocity at the end of the breakup process have an inverse dependence. This means that higher

392 velocity droplets are smaller than lower velocity droplets. The exact droplet size and velocity depends on

393 the wave specification, vessel velocity, wind velocity, and the quality of the impact. By knowing the range

394 of velocities and sizes of the droplets at the highest level of the bow, and considering the velocity direction

395 of droplets nearly parallel with the bow, a wind velocity of 11 m/s, and a vessel velocity of 2.83 m/s, the

396 same as the situation of the MFV of the Sea of Japan which is reported by Borisenkov et al. (1975), the

397 effect of these variables on the spray cloud and LWC can be examined. Table 1 shows the values for the
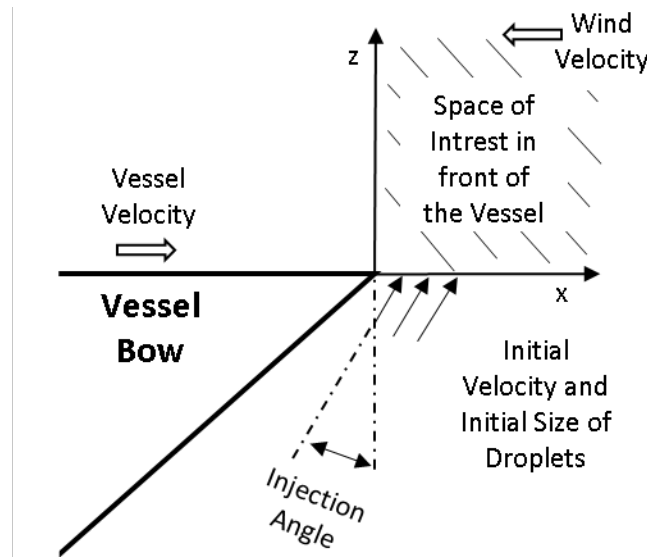
398 droplet trajectory.

399

400 Table 1. Working conditions of droplet trajectory in front of the vessel

Parameters	Reference Values	Unit
Initial Velocity of Droplets	0-40	m/s
Droplets Diameter	0-7000	μm
Injection Angle	20	Degree

401

19

402   Figure 7 shows a schematic view of the bow, injection location and angle of droplets, wind velocity,

403   and vessel velocity. The coordinate system is attached to the vessel and the origin is on the highest point

404   of the bow in front of the vessel. As mentioned, this study is limited to the survey of spray creation in

405   front of the vessel. The droplet trajectory on the vessel is beyond the scope of this research. The space of

406   interest is confined between the positive coordinate axes of x and z.

407

408

409   Fig. 7. Schematic view of the bow and the variables

410

411   The first output of the droplet trajectory will be the dispersion of a spray cloud in front of the vessel.

412   Figure 8 shows the development of a spray cloud over time. The spray cloud will cover the entire front of

413   a vessel in less than 0.48 s. At this point, the spray is not at its maximum height over the vessel. The spray

414   cloud can further extend upwards on the vessel and the geometry of the deck can affect it.

415   The maximum counter-direction horizontal movement of the spray cloud in front of the vessel is

416   about $0.45\ m$. The spray cloud is extended vertically very rapidly. After $0.16\ s$, the height of the spray

417   reaches about $1.7\ m$ and, at $0.24\ s$, it reaches a height of $2.7\ m$. At $0.32\ s$, the spray has moved vertically

418   just $0.8\ m$, to a height of $3.5\ m$. At a time of $0.4\ s$, the spray cloud is extended completely in the vertical

419   direction and it reaches the maximum height in front of the vessel. In the next $0.08 \, s$, the height remains

420   constant, but some slow droplets complete their movement towards the vessel and reach the deck, and

421   consequently the pattern of the spray cloud in front of the vessel is complete.

422

423

$t = 0.16 \, s$ $t = 0.24 \, s$ $t = 0.32 \, s$ $t = 0.40 \, s$ $t = 0.48 \, s$
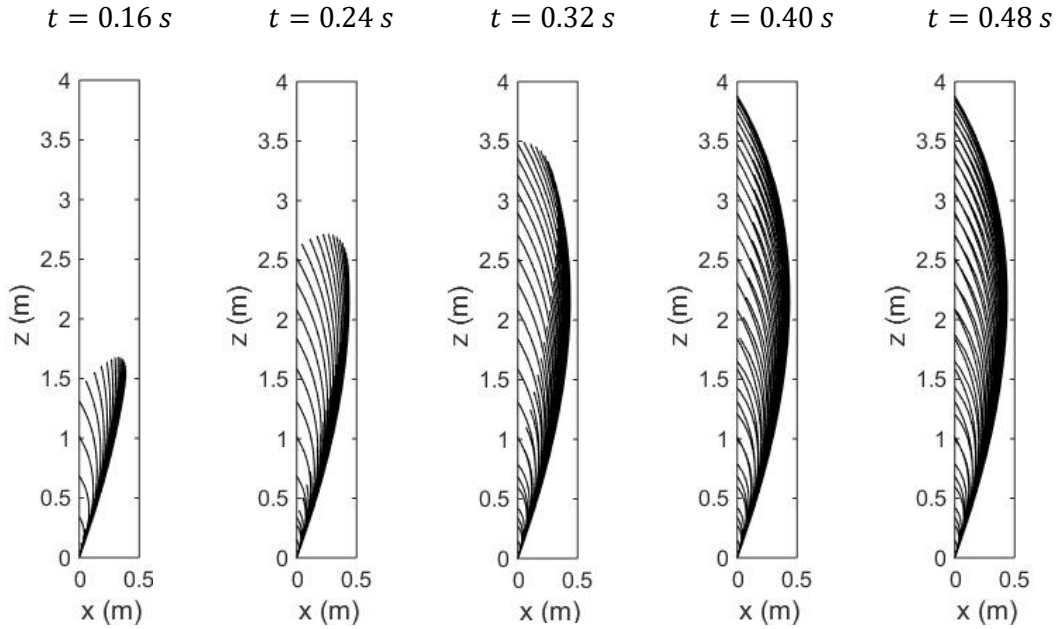
424   Fig. 8. Spray cloud development in front of a vessel. Vertical development versus horizontal

425   development in front of a vessel (Compatible with the coordinate axis of Fig. 7)

426

427   The liquid water content from the field observations can be used as a reference to check the

428   numerical solution. Figure 9 shows a comparison between the numerical results and the LWC reported by

429   Borisenkov et al. (1975). The proposed relation that represents the liquid water content is given by

430               $$w = 24.2 \times \exp(-0.55z) \qquad gr_{water}/m^3{}_{air} \qquad (10)$$

431   where z is the elevation above the deck of MFE (Zakrzewski, 1987) and w is the LWC.

432
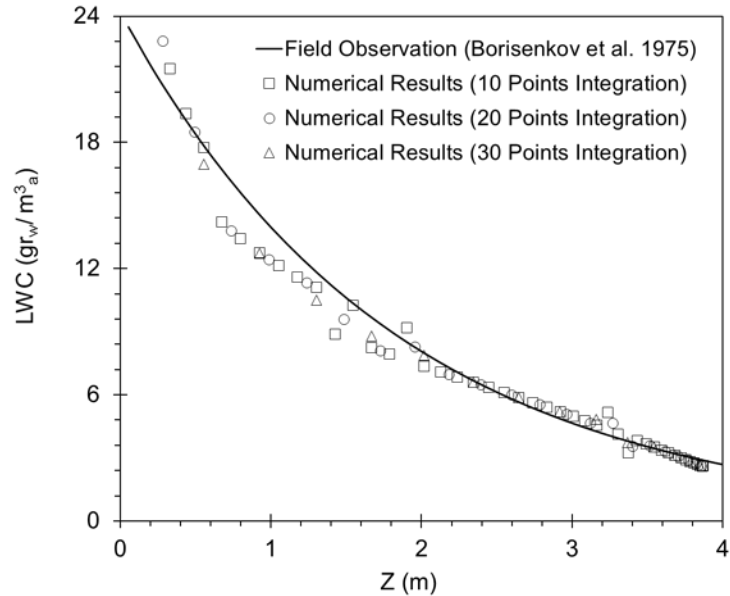
433

434   Fig. 9. Comparison of liquid water content of the numerical approach and a fit to the field observations

435   by Borisenkov et al. (1975)

436

437   There are various numbers of droplets with different sizes and velocities at every point of the spray

438   cloud. The numerical results are obtained based on integration of the properties of this inhomogeneous

439   discrete phase of water droplets in the vertical direction. This integration requires the definition of space

440   intervals and points on the relevant domain. Figure 9 shows the numerical results in different cases of

441   integration intervals and points. Due to the integration on the discrete phase of water droplets, the

442   obtained LWCs may not be smooth curves. The quality of the numerical curves depends on the number

443   of intervals and points on the subdivided ranges. Some points on the curves are the result of the

444   inhomogeneous distribution of droplets and also the integration intervals and points. Figure 9 shows that

445   increasing the integration points can refine these regions and also reduce the number of resultant data

446   on the curves.

447   The numerical results are aligned with the field observations. They almost match the exponential

448   behaviour of the experimental results. For the higher altitudes, they are well matched and for lower

                                                    22

449 altitudes, some small differences exist. The main result of this comparison emphasizes that the

450 distribution of sizes, which is inversely proportional to the distribution of velocities, is compatible with the

451 exponential behaviour of vertical distribution of the LWC. In the next section, it will be shown that the

452 other relations between the sizes and velocities cannot yield an exponential function and the most valid

453 relation is an inversely proportional relation.

454

5. Sensitivity Analysis

456 A sensitivity analysis was conducted to determine how sensitive this model is to changes in the value of

457 the input parameters. By showing how the model behavior responds to changes in input parameter

458 values, the sensitivity analysis is a useful tool in model building as well as in model evaluation. The first

459 test will assess the sensitivity of the model to various size-velocity dependencies of the droplets. Referring

460 to past studies (Lozowski et al., 2000; Zakrzewski, 1987; Shipilova et al., 2012; Horjen, 2013; Kulyakhtin

461 and Tsarau, 2014) and assumptions for choosing the initial velocity and size in the spray cloud, it is possible

462 to categorize the assumptions and other possible cases to some individual categories. There are four

463 individual cases for the dependence of velocity on the size of droplets. The first case is an inverse

464 dependence, which has high-velocity, small-sized droplets and low-velocity, large-sized droplets. The

465 second case is the opposite of the first case. This case, which will be named the co-direction dependence,

466 considers high-velocity, large-sized droplets and low-velocity, small-sized droplets. The third case is a

467 constant velocity and arbitrary droplet size, and the fourth case is a constant droplet size and arbitrary

468 droplet velocity. It will be shown that, except in the first case, which has been chosen for this study, the

469 other cases do not yield an acceptable LWC curve.

470 Figure 10 shows the response of the model to various inputs of size-velocity dependence. The co-

471 direction case is the least appropriate case and predicts a nearly linear curve with an opposite slope with

472 respect to the field observation data. The other case occurs when velocity is constant, which predicts a

23

473   nearly parabolic curve. Another scenario is when the droplet size is constant. This cannot be adequately

474   fit to an exponential correlation of the field observation. The curve is approximately horizontal, and

475   therefore it is not a suitable case to be chosen.

476
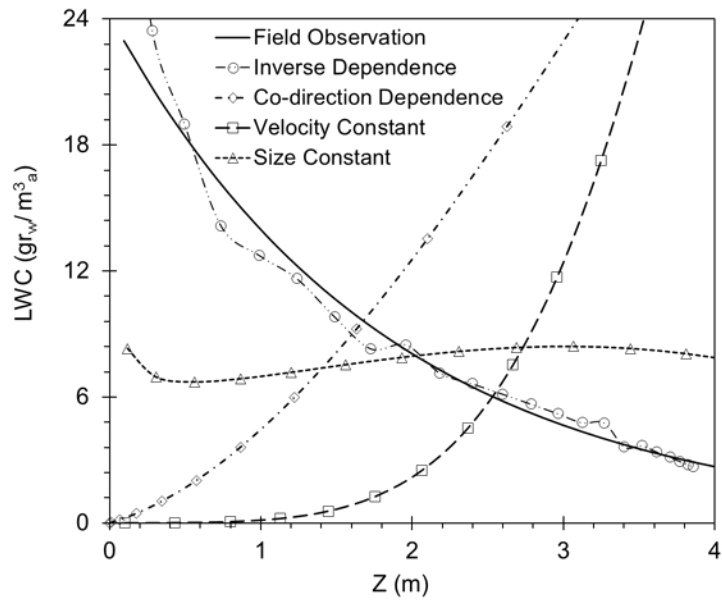
477

478   Fig. 10. Sensitivity of the model to various size-velocity dependences

479

480   As shown in Fig. 10, the assumption of a constant velocity and size cannot adequately yield the

481   exponential form of the LWC formula. The co-direction dependence is another inappropriate assumption

482   for droplet size and velocity information. This analysis shows that the previous assumptions are not

483   suitable. The other significant conclusion of this analysis is the importance of determining the distribution

484   of size and velocity instead of assuming a constant velocity and size. The only acceptable case is an inverse

485   velocity-size dependence. This case can be fit to an exponential curve and is in alignment with the field

486   observation reports. The sensitivity analysis of size-velocity dependence shows that the model is highly

487   sensitive to the size-velocity dependence. This means the only suitable case of size-velocity dependence

488   in wave-impact sea spray is inverse dependence. This sensitivity analysis is good evidence for the necessity

489   of the inverse size-velocity dependence in the wave-impact breakup.

490   The other parameters that test the sensitivity of the model are the maximum velocity of droplets,

491   maximum size of droplets, and injection angle. The various degrees of these parameters are shown in

492   Table 2. In each case of sensitivity analysis the response of the model is evaluated by varying a parameter

493   in the mentioned range of Table 2. The other parameters are kept at the reference values.

494

495   Table 2. Various amounts of input data for sensitivity analysis

Parameters	Unit	Range of Values for Sensitivity Analysis				
				Reference		
Initial Velocity of Droplets	m/s	0-20	0-30	0-40	0-50	0-60
Droplet Size (Diameter)	μm	0-5000	0-6000	0-7000	0-8000	0-9000
Injection Angle	Degree	10	15	20	25	30

496

497   Figure 11 shows the response of the model to various initial velocities. This test is conducted by

498   using the reference values of droplet size and injection angle. The model is very sensitive to the variation

499   of droplet velocities. The most considerable response of the system to a variation of the maximum initial

500   velocity of droplets appears in the higher altitudes. In the case of lower velocities, droplets create a short

501   cloud spray and therefore the LWC is zero for the high altitude. The model is more sensitive to lower

502   velocities than to higher ones. At high velocities, the maximum deviation is less than 8 percent but for low

503   velocities the deviation is more than 50 percent. For all cases, the LWC for the heights of less than 1 m are

504   very close to each other, but by increasing the height, the lower velocity cases start to diverge.

505

25
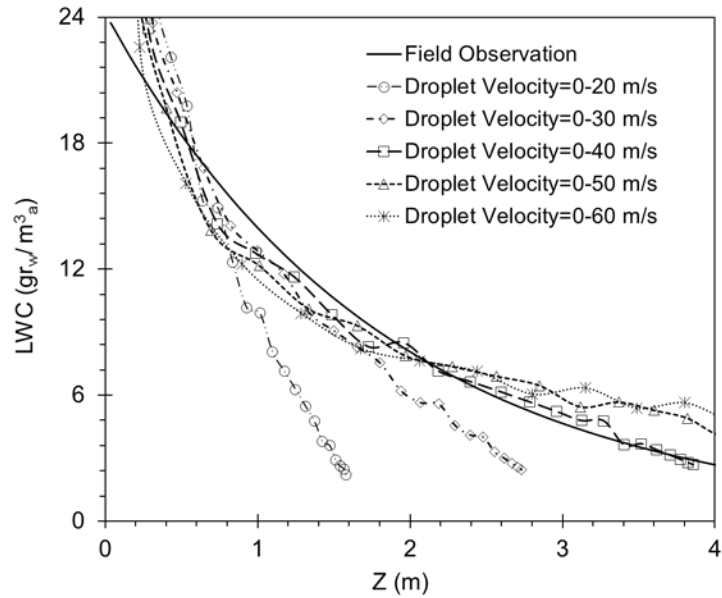
Fig. 11. Sensitivity response of model to various initial velocities

The droplet size is the other parameter that can test the sensitivity of the model. Figure 12 shows the response of the model to this parameter. Increasing the droplet size results in an increase of LWC. The system is more sensitive to larger droplets than to smaller droplets. The volume of water is proportional to the third power of the droplet diameter and it can be the reason for the high sensitivity of the model to bigger droplets. When decreasing the maximum size of the droplets, they cannot travel as high as the reference value case because of the drag force. The drag force affects the small droplets more easily, and they will be in the wind direction after a short time. Therefore they cannot reach the highest altitude.
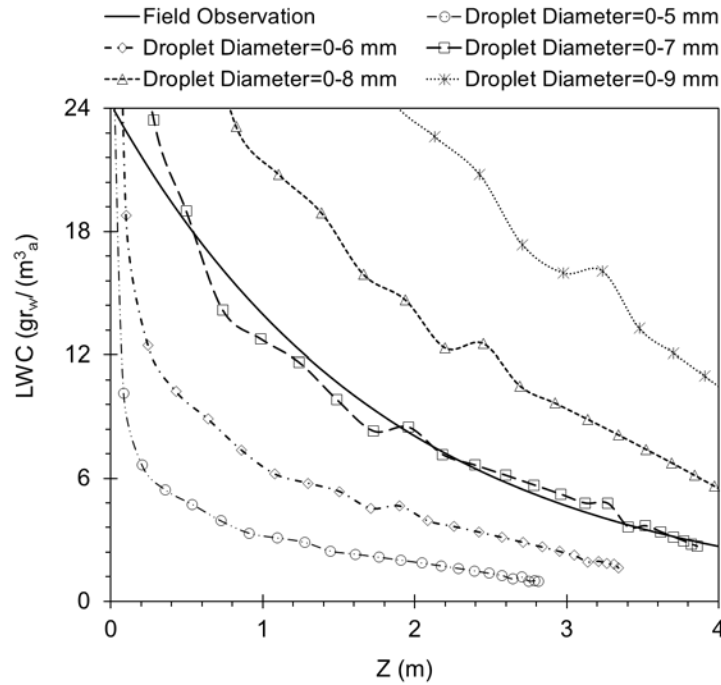
Fig. 12. Sensitivity response of model to droplet sizes
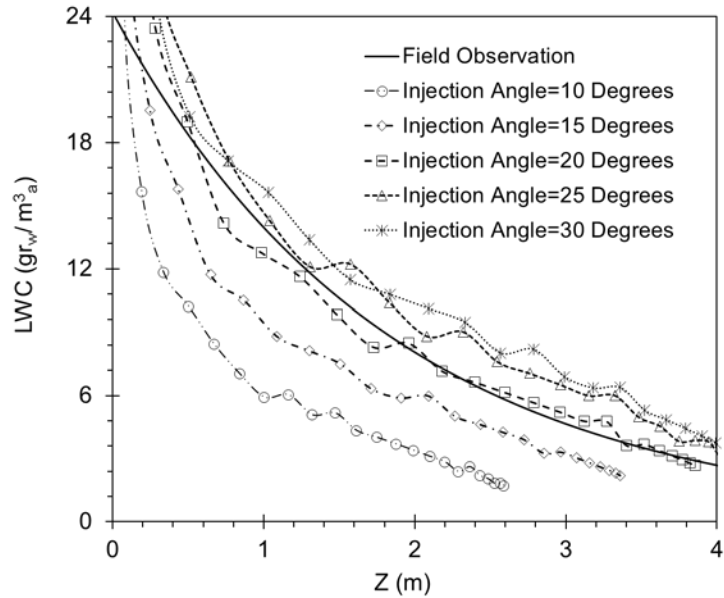
The sensitivity of the model to injection angles is the last part of the sensitivity analysis. Figure 13 shows the response of the model to this parameter. The model is more sensitive to smaller injection angles than to greater angles. In comparison to the higher injection angles, the smaller injection angles create lower values of horizontal components and higher values of vertical components of the initial velocity of droplets. The greater injection angles result in lower values of LWC in comparison to that of smaller injection angles. In addition, due to smaller horizontal components of the initial velocity of droplets, the droplets take a shorter path and consequently arrive on the deck before reaching the higher altitudes. Therefore the LWC of heights greater than 2.6 m for the injection angles of 10 degrees is zero. This means that decreasing the injection angle decreases the effective height of the LWC. The greater injection angles yield higher values for the LWC in comparison to the reference value.

Fig. 13. Sensitivity analysis of model to various injection angles

Generally the sensitivity of the model to the injection angle is less than the sensitivity of the model to droplet size or droplet velocity. The model is very sensitive to droplet sizes and the LWC is affected by changing the sizes strongly. The velocity range is the case that can affect the effective height of the LWC. Increasing the maximum velocity increases the height of the LWC and vice versa.

6. Conclusions

A new model for the prediction of the characteristics of wave-impact sea spray in front of a vessel was developed. The sheet breakup and droplet breakup in front of the vessel bow showed that there is a significant dependence between the sizes and velocities of resulting droplets after breakup. High-velocity droplets tend to split into fine droplets and low-velocity droplets tend to keep their size. This makes a size-velocity connection in the droplets which are injected into the atmosphere in front of a vessel. At the injection points, next to the highest points of the bow, the bigger droplets have lower velocities and vice versa. By using the droplet trajectory and considering the vessel velocity and wind velocity, the spray cloud

28

546   in front of the vessel can be predicted. The drag force, added mass force, and body force are effective

547   forces in this analysis. The wave-impact sea spray is expanded in front of the vessel in 0.48 s. The LWC is

548   calculated by considering the droplet arrangement, size, and velocity at the arrival section in front of the

549   vessel.

550   Sensitivity analyses show that the model is very sensitive to size-velocity dependence. Co-direction

551   dependence for the size and the velocity, independence of droplet size from velocity, and independence

552   of droplet velocity from size, will result in unacceptable values of the LWC. The inverse dependence

553   between size and velocity is the only dependence that can adequately predict the correct value of the

554   LWC. The sensitivity analysis shows that the system is very sensitive to small injection angles, big droplets,

555   and low-velocity droplets. The proposed inverse size-velocity dependence for the injected droplets in the

556   atmosphere in front of the vessel is a useful new model that can fill a knowledge gap about the size and

557   velocity of droplets due to the impact of a wave on a bow. This proposed model was verified by comparing

558   it to the LWC measured by Borisenkov et al. (1975). By using this new model, a more accurate calculation

559   of the water impact across a vessel can be achieved.

560

561   ## Acknowledgments

564

565   ## References

566   Adams, T.N., Frederick, W.J., Grace, T.M., Hupa, M., Lisa, K., Jones, A.K., Tran, H., 1977. Kraft Recovery

567   Boilers. TAPPI Press.

568   Ahmed, M., Ashgriz, N., Tran, H.N., 2009. Break-Up Length and Spreading Angle of Liquid Sheets Formed

569   by Splash Plate Nozzles. Journal of Fluid Engineering, 131, 1-9.

570   Ashgriz N., Washburn R., Barbat T., 1996. Segregation of drop size and velocity in jet impinging splash-

571   plate atomizers. International Journal of Heat and Fluid Flow, 17 (5), 509–516.

572   Borisenkov, Y.P., Zablockiy, G.A., Makshtas, A.P., Migulin, A.I., Panov, V.V., 1975. On the approximation of

573   the spray cloud dimensions. Arkticheskii I Antarcticheskii Nauchno-Issledovatelskii Instit. Trudy 317.

574   Leningrad: Gidrometeoizda (in Russia), pp. 121-126.

575   Bussmann, M., Chandra S., Mostaghimi J., 2000. Modeling the splash of a droplet impacting a solid surface.

576   Phys. Fluids 12, 3121.

577   Dehghani, S.R., Saidi, M.H., Mozafari, A.A., Ghafourian, A., 2009. Particle Trajectory in a Bidirectional

578   Vortex Flow. Particulate Science and Technology, 27, 16–34.

579   Dehghani, S.R., Saidi, M.H., Mozafari, A.A., Soleimani, F., 2013. Particle Dispersion Dependency on the

580   Entrance Position in Bidirectional Flow. Particulate Science and Technology, 31, 576–584.

581   Forest, T.W., Lozowski, E.P., Gagnon, R., 2005. Estimating Marine Icing on Offshore Structures using

582   RIGICE04. IWAIS XI, Montréal, June 2005.

583   Horjen, I., 2013 Numerical modeling of two-dimensional sea spray icing on vessel-mounted cylinders, Cold

584   Regions Science and Technology, 93, 20–35.

585   Horjen, I., Carstens, T., 1989. Numerical modelling of the sea spray icing on vessels. In Proc. 10th Int. POAC

586   Conf., Lulea, Sweden, vol. 3, pp. 694-704.

587   Greco, M., Bouscasse, B., Lugni, C., 2012. 3-D seakeeping analysis with water on deck and slamming. Part

588   2: Experiments and physical investigation. Journal of Fluids and Structures, 33, 148-179.

589   Greco, M., Lugni, C., 2012. 3-D seakeeping analysis with water on deck and slamming. Part 1: Numerical

590   Solver. Journal of Fluids and Structures, 33, 127-147.

591   Gu, H.B., Qiana, L., Causona, D.M., Minghama, C.G., LinbNumerical P., 2014. Simulation of water impact

592   of solid bodies with vertical and oblique entries. Ocean Engineering. 75, 128-137.

593   Ingebo, D., 1984. Atomization of liquid sheets in high pressure air flow. NASA-Lewis Research Center,

594   Cleveland, OH.

595   Kaspenberg, G.K., 2011. Slamming of ships: where are we now? Phil. Trans. R. Soc. A, 369, 2892-2919.

596   Kulyakhtin, A., Tsarau, A., 2014. A time-dependent model of marine icing with application of

597   computational fluid dynamics. Cold Regions Science and Technology, 104–105, 33–44.

598   Lozano. A., García-Olivares, A., Dopazo, C., 1998. The instability growth leading to a liquid sheet breakup.

599   10 (9), 2188-2197.

600   Lozowski, E.P., Szilder, K., Makkonen, L., 2000. Computer simulation of marine ice accretion. Royal Society,

601   358, 2811-2845.

602   Makkonen, L., 1984. Atmospheric icing on sea structures. US Army Corps of Engineers, Cold Regions

603   Research & Engineering Laboratory, CRREL MONOGRAPH 84.2.

604   Ryerson, C.C., 1995. Superstructure spray and ice accretion on a large U.S. Coast Guard cutter.

605   Atmospheric Research, 36 (3–4), 321–337.

606   Ryerson, C.C., 2011. Ice protection of offshore platforms. Cold Regions Science and Technology, 65 (1),

607   97–110.

608   Sarchami, A., Ashgriz, N., Tran, H., 2010. An atomization model for splash plate nozzles. AIChE Journal, 56

609   (4), 849–857.

610   Sazhin, S., 2014. Droplet and sprays. Springer-Verlag London.

611   Shipilova, O., Kulyakhtin, A., Tsarau, A., Libby, B., Moslet, P.O., Loset, S., 2012. Mechanism and Dynamics

612   of Marine Ice Accretion on Vessel Archetypes, OTC-23762-MS, OTC Arctic Technology Conference, 3-5

613   December, Houston, Texas, USA.

614 Zakrzewski, W.P., 1987. Splashing a ship with collision-generated spray. Cold Regions Science and

615 Technology, 14 (1), 65–83.

616 Zakrzewski, W.P., Lozowski, E.P., 1988. Estimating the extent of the spraying zone on a sea-going ship.

617 Ocean Engineering. 15 (5), 413–429.